Alignment of Rod-Shaped Single-Photon Emitters Driven by Line Defects in Liquid Crystals

*Laurent Pelliser, Mathieu Manceau, Clotilde Lethiec, Delphine Coursault, Stefano Vezzoli, Godefroy Leménager, Laurent Coolen, Massimo DeVittorio, Ferruccio Pisanello, Luigi Carbone, Agnes Maitre, Alberto Bramati, and Emmanuelle Lacaze**

Arrays of liquid crystal defects—linear smectic dislocations—are used to trap semiconductor CdSe/CdS dot-in-rods which behave as single-photon emitters. Measurements of the emission diagram are combined together with measurements of the emitted polarization of the single emitters. It is shown that the dot-in-rods are confined parallel to the linear defects to allow for a minimization of the disorder energy associated with the dislocation cores. It is demonstrated that the electric dipoles associated with the dot-in-rods, tilted with respect to the rods, remain oriented in the plane including the smectic linear defects and perpendicular to the substrate, most likely due to dipole/dipole interactions between the dipoles of the liquid crystal molecules and those of the dot-in-rods. Using smectic dislocations, nanorods can consequently be oriented along a unique direction for a given substrate, independently of the ligands' nature, without any induced aggregation, leading as well to a fixed azimuthal orientation for the dot-in-rods' dipoles. These results open the way for the fine control of nanoparticle anisotropic optical properties, in particular, fine control of single-photon emission polarization.

1. Introduction

Control of single-photon emitters is a major objective in the field of nanophotonics.[1] The synthesis of colloidal semiconductor inorganic nanocrystals having specific light-emission properties has been providing important advances in this field. In particular, recent developments in synthesis methodologies, fully compatible with standard nanofabrication technologies have enabled a superior control on nanocrystals composition and morphology. Rod-shaped nanocrystals showing pronounced polarization, behaving as emitting linear dipoles, have been obtained.[2–4] The encapsulation of a spherical core into a rod-like shell[5] resulted in nonblinking inorganic single-photon emitters,[6] hereafter referred to as dot-in-rods (DRs). Moreover, it has been recently shown that, by increasing the thickness of the shell, it is possible to greatly suppress photoluminescence blinking and to improve DRs overall photostability, while keeping a low probability of multiphoton emission.[7] Such features are of primary importance when nanocrystals are used in applications demanding a control of photons' polarization, such as coupling with complex photonic cavities[8,9] or quantum cryptography.[10] The control of the polarization of the emitted light also requires the capacity to control the particle orientation. However, technologies aimed at guiding nanocrystal orientation at the single particle level are still poorly discussed in literature.

Aligned nanoparticles have been obtained through mechanical rubbing,[11] short-range interactions,[12,13] or patterned substrates.[14] Liquid crystal-like structures, composed of a large number of elongated nanocrystals assembled in multilayers have also been evidenced on both solid substrates[15–18] and water films.[18–20] Orientation and positional

L. Pelliser, Dr. C. Lethiec, Dr. D. Coursault, Dr. L. Coolen, Prof. A. Maitre
Dr. E. Lacaze
CNRS, UMR 7588
Institut des NanoSciences de Paris (INSP)
4 place Jussieu, F-75005 Paris, France
E-mail: emmanuelle.lacaze@insp.jussieu.fr

L. Pelliser, Dr. C. Lethiec, Dr. D. Coursault, Dr. L. Coolen, Prof. A. Maitre
Dr. E. Lacaze
Institut des NanoSciences de Paris (INSP)
Sorbonne Universités
UPMC Univ Paris 06, UMR 7588
4 place Jussieu, F-75005 Paris, France

Dr. M. Manceau, Dr. S. Vezzoli, Dr. G. Leménager, Prof. A. Bramati
Laboratoire Kastler Brossel, Collège de France
UPMC-Sorbonne Universités, CNRS, ENS-PSL
Research University
4 place Jussieu Case 74, F-75005, Paris France

Dr. S. Vezzoli
Centre for Disruptive Photonic Technologies
Nanyang Technological University
637371, Singapore

Prof. M. DeVittorio
Dipartimento di Ingegneria dell'Innovazione
Università del Salento
Via per Monteroni, 73100 Lecce, Italy

Prof. M. DeVittorio, Dr. F. Pisanello
Center for Biomolecular Nanotechnologies @Unile
Istituto Italiano di Tecnologia (IIT)
Via Barsanti, 73010 Lecce, Italy

Prof. M. DeVittorio, Dr. L. Carbone
National Nanotechnology Laboratory (NNL)
CNR-Istituto Nanoscienze
Via Arnesano km 5, 73100 Lecce, Italy

DOI: 10.1002/adfm.201403331

ordering of CdS and CdSe nanorods have been obtained through the utilization of a local electric field, exploiting their intrinsic electric dipole moments.[18,21–23] However, single nanorods are rarely observed once aligned onto the substrate: only average optical properties can be inferred from these experiments. The fluorescence polarization of a number of single DRs has been measured but not for aligned ones.[5,6,24,25] In order to obtain a macroscopic organization and orientation of single nanorods onto a substrate, the use of anisotropic matrices working as hard or soft templates offers a promising experimental alternative, as shown for polymer matrices,[26,27] which can be stretched,[5,28] as shown for DNA molecules[29] and carbon nanotubes,[30] both of which can be used as oriented particles.

An increasing number of works is also devoted to the use of anisotropic matrices made of liquid crystals.[31–36] Cholesteric liquid crystals have been used to control the circular polarization of single quantum dots.[37] Nematic liquid crystals have been used to orient single dye molecules, either parallel or perpendicular to the nematic director, depending on the molecular shape.[37,38] In nematic liquid crystals, nanorods can be oriented as well, either parallel or perpendicular to the liquid crystal director, depending on the liquid crystal ability to anchor the nanorod surface,[39,40] with the possible help of magnetic fields.[41,42] However, a serious drawback met in the use of most of thermotropic liquid crystals is associated with the induced aggregation of the nanorods.[36,43,44] This aggregation is due to the distortions and disorder induced in the liquid crystal around most of the nanoparticles, which become reduced if the nanoparticles are aggregated.[36,45] In nematic liquid crystals, the best method to prevent aggregation of nanorods is to graft specific ligands around the nanorods in order to allow for a weak anchoring of the liquid crystal molecules.[46,47] Weak anchoring indeed prevents the formation of liquid crystal defects and thus prevents aggregation. For semiconductor nanorods embedded in liquid crystals, average orientations parallel to the nematic director have been evidenced but, to the best of our knowledge, again only ensemble anisotropic emission properties have been studied.[22,46,48,49]

Herein, we demonstrate that linear arrays of smectic liquid crystal defects behave as a "smart" matrix to govern the positional and directional ordering of nanorods. Single nanorods can be manipulated and oriented along the defects, along a unique direction for a given substrate. This avoids any liquid crystal-induced aggregation of nanorods, independently of the ligand's nature. We evidence the phenomenon with DRs, single-photon emitters, at the single particle level. Statistical analysis of the inplane orientation of the single DRs leads to a unique orientation with 8° of standard deviation, leading therefore to a fine control of single-photon emission polarization.

Although we use core-shell CdSe/CdS DRs as a model system, the technology can be easily extended to a wide class of anisotropic nano-objects. The choice of these particles was dictated by their geometrical properties – a 1D shape used in combination with the linear liquid crystal structures described later on – in order to obtain orientation of the rods; their quantum properties – they behave as single-photon emitters[7] – and their polarized emission,[6] in order to control the polarization of the emission of single emitters.

2. Results

Two different experimental approaches have been used for rubbing the PVA-coated substrates. The first method consisted in rubbing the substrates through a hand-operated procedure, in our case by using cotton sticks, achieving aligned zones, parallel from each other, but extended over small-scale areas only (of the order of several dozens of micrometers—see **Figure 1**a). These areas are separated by disordered zones, without preferred liquid crystal orientation and thus without oriented oily streaks. The second method uses a rubbing machine providing almost no disordered zones, essentially showing regular stripes (Figure 1b) aligned along a single direction over the whole sample surface, this direction being perpendicular to the rubbing direction. In Figure 1c, we plot the fluorescence intensity $I(\alpha)$ emitted by three individual DRs, as a function of the polarization analysis angle α, for the manually rubbed sample, cf. Figure 1a (thickness 140 nm). For each DR, the measured intensity shows the typical $\cos^2(\alpha-\Phi)$ dependence of Equation (1), as shown from the comparison between raw data and a $\cos^2(\alpha-\Phi)$ fit. If we compare two DRs localized on two oriented areas (DRs B and C on Figure 1a), we obtain a similar phase of $I(\alpha)$, moreover, with an intensity maximum at $\alpha = 0°$, corresponding to the stripes orientation (Figure 1a). If we compare them with one DR on a disordered area (DR A on Figure 1a), different $I(\alpha)$ phases are obtained. It brings the conclusion that the fluorescence polarization is maximum in a well-defined direction parallel to the stripes, only when the DRs are localized in oriented oily streaks. The same result is obtained for the $I(\alpha)$ curves of the DRs of the homogeneously rubbed sample (red circles in Figure 1b). In Figure 1d, the histogram of the angle values corresponding to the fluorescence maximum for the 20 DRs of Figure 1b is presented. A common phase value for the different DRs appears clearly, with an average of $\Phi = 29.9°$ and a standard deviation of 5.6°. This average value is the same than the stripes orientation, visible on optical microscopy (Figure 1b), with a measurement uncertainty of ±1°. If now we consider a larger number of single DRs located in two different samples of similar 8CB thickness of the order of 100 nm (52 DRs), we find again a well-defined value for the fluorescence anisotropy, corresponding to the stripes orientation, with a standard deviation of 8°. This demonstrates that, not only the DRs fluorescence share a common orientation, but also that this orientation is the one of the oily streaks defects.

The hypothesis of an influence of the liquid crystal birefringence on the fluorescence polarization anisotropy of the DRs can be ruled out for two reasons. First, it has been shown recently that the excitation anisotropy of DRs is mainly affected by the nature of the ligands directly around the DRs.[25] Second, several ensemble measurements of polarization anisotropy have been conducted within nematic liquid crystals.[22,46,48,49,50] This led to a maximum fluorescence parallel to the nematic director (extraordinary index) in contrast with the present case. In smectic oily streaks, Figure 1 shows that the fluorescence is maximum for a polarization along the stripes, in other words perpendicular to the smectic director and corresponding to the ordinary index of the 8CB. The fluorescence is minimum for a polarization perpendicular to the stripes, corresponding to a combination between ordinary and extraordinary index.

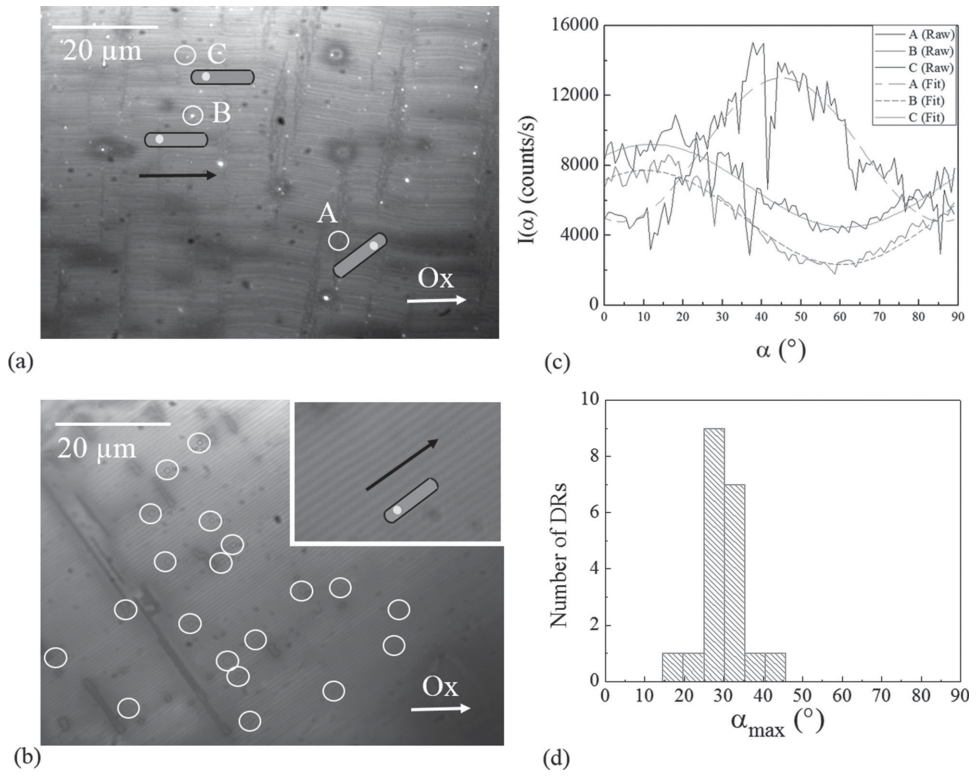

Figure 1. a) Superposition of the pictures obtained in optical microscopy (oily streaks) and fluorescence microscopy (DRs) on a 8CB sample (140 nm thick) with imperfect PVA polymer rubbing. Three specific DRs are chosen for observation. The arrow indicates the axis of the oily streaks, the inplane orientation of the dipoles (as deduced from (c)) being shown with the rod-like icons. b) 130-nm-thick 8CB smectic oily streaks observed through optical microscopy with the PVA rubbing performed by means of a rubbing machine. The position of the DRs is found in the smectic oily streaks, via fluorescence microscopy and highlighted by white circles in the picture—the inset shows a zoom of size 13.5 × 9 µm. The arrow indicates the axis of the oily streaks, the in-plane orientation of the dipoles (as deduced from (1d)) being shown with the rod-like icon. c) Overlay of the photoluminescence intensity emitted by three DRs shown in (1a) as a function of the polarization analysis angle α. A fit with a $\cos^2(\alpha-\Phi)$ function is superimposed to the three curves. d) Histogram of the angle value corresponding to the fluorescence maximum obtained from the $\cos^2(\alpha-\Phi)$ fit for the 20 DRs measured in (1b).

For both nematic and smectic liquid crystals, the fluorescence anisotropy can be attributed to an in-plane orientation of the DR dipole, imposed by the liquid crystal orientation and not to an optical birefringence effect. In nematic liquid crystals, the fluorescence polarization anisotropy is related to an orientation of the nanorods parallel to the liquid crystal director, as it is most often the case due to the liquid crystal anchoring at the nanorods surface.[22,39,40,46,48–50]In smectic oily streaks, the in-plane projection of the DRs dipole is oriented parallel to the oily streaks stripes (scheme of the dipoles on Figure 1). It is thus parallel to the linear defects, and, perpendicular to the liquid crystal director (**Figure 2**). This suggests a different physical mechanism for the aligning phenomenon in smectic oily streaks compared to oriented nematic liquid crystals.

The dipole orientation with respect to the smectic texture is confirmed by a defocused microscopy technique,[6,49] already used to assess DRs dipole orientation.[6,51] It has been employed by means of an oil immersion microscope objective with high numerical aperture (NA 1.4) positioned 500 nm away from the focal point. As shown in **Figure 3**, bright and dark arcs appear around each original focused spot, confirming the dipolar nature of the emission.[6,48,51–54] These defocusing patterns give information on both inplane and out-of-plane dipole orientation,[52–54] if it is taken into account that they are influenced by several other parameters such as NA of the objective, dielectric environment (liquid crystal and air interface) and that they are significantly dependent on the distance between the objective focal plane and the sample.[48,55,56] For linear dipoles, defocused images displaying lobe patterns with a single symmetry axis correspond to dipoles neither horizontal nor vertical, but rather tilted with respect to the substrate. By connecting the two minima of the internal arcs, the dipole inplane component

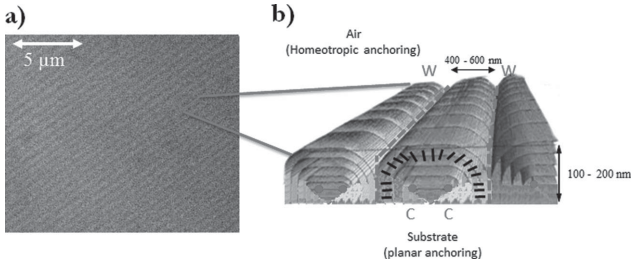

Figure 2. a) Oily streaks observed by optical microscopy on a sample 120 nm thick, viewed from the top. b) Scheme of the oily streaks with the smectic layers schematically shown in 3D and the molecules' orientation indicated in black. The centers of curvature are indicated dots (marked as C for the central hemicylinder), and the walls between the hemicylinders, W, are highlighted with dashed lines.

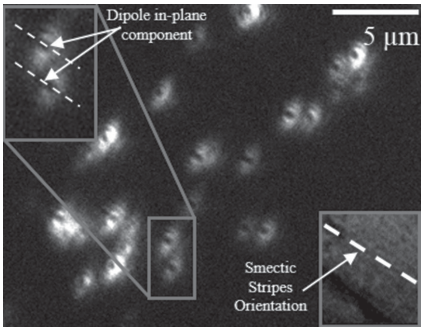

Figure 3. Main) Photoluminescence of DRs illuminated with the 436 nm band of a Hg lamp in defocused configuration: the objective is defocused by setting the focal plane 500 nm far from the DR; the image is taken after filtering out the reflection with a high-pass filter to keep the photoluminescence. Inset-left) Zoom on two defocusing spots. Inset-right) (5 × 6 µm) In absence of high-pass filter and in focused configuration, the oily streaks are observed with the same source.

orientation can be assessed: as shown in the upper-left inset of Figure 3, it is parallel to the oily streaks axis, highlighted in the bottom-right inset. This confirms the result gained from Figure 1. Importantly, again, this specific orientation is common to the majority of the isolated DRs within the rubbed area (see Figure S3, Supporting Information).

In Figure 3, the asymmetry of the defocusing spots shows a tilt of the DRs dipoles out of the substrate plane. In order to supplement these defocusing measurements, we have considered the degree of linear polarization δ for the emitted light of the single DRs in the liquid crystal matrix: $\delta = (I_{max}-I_{min})/(I_{max}+I_{min})$. I_{max} and I_{min} are obtained from polarization analysis curves as in Figure 1c, after careful background subtraction. For DRs approximated by linear dipoles,[7,28,51] δ can be theoretically calculated taking into account the dielectric nature of the environment of the dipole.[52] The theoretical curve of the degree of polarization δ as a function of the dipole out-of plane tilt, θ, with respect to the microscope optical axis (normal to the substrate), is shown on **Figure 4**a for a linear dipole located in a 1.5 index medium, whose emission is collected by a 0.95 NA air objective.[52] $\delta \approx 1$ for $\theta = 90°$, which is a horizontal dipole and $\delta = 0$ for $\theta = 0°$, which is a vertical dipole.

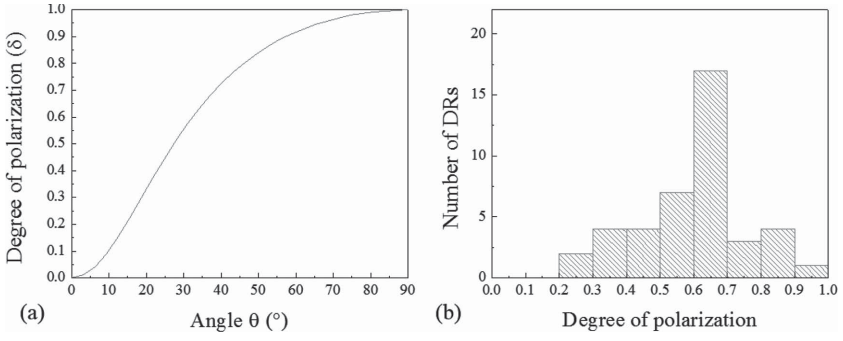

Figure 4. a) Degree of polarization of a linear dipole located in a 1.50 refractive index medium, whose transmitted emission is collected by a 0.95 NA air objective, as a function of its out-of-plane angle θ. This curve does not depend on the distance to the interface. b) Histogram of the measured degrees of polarization for 42 DRs in 8CB liquid crystal films of thickness around 100 nm.

We measured the degrees of polarization of 52 DRs dispersed in two similar samples of liquid crystal thickness around 100 nm, including the one of Figure 1b. We removed, for this measurement, the signal of the DRs not aligned within 6° to the liquid crystal stripes and most probably corresponding to nanoparticles of different shapes (see TEM image displayed in Figure S2, Supporting Information).[25] The obtained histogram of degree of polarization, for the 42 remaining DRs, is shown on Figure 4b. A well-defined peak is evidenced between 0.6 and 0.7. As shown by Figure 4a, this limited value of polarization is consistent with the out-of-plane tilt of the emitter dipoles evidenced on the defocalization results of Figure 3. It may also be associated with DRs not fully polarized, as shown in a number of ensemble measurements,[5,24,25] in particular for CdSe/CdS DRs of similar ratio core diameter over DR diameter, the role of this last parameter being recently underlined.[46] The additional broad distribution of degrees of polarization observed on Figure 4b may be related to the dispersion of size and shape of the DRs (see Figure S2, Supporting Information), to the distribution of core shape,[24,25,57,58] together with possible distribution of dipole out-of-plane orientation.

3. Discussion

In a similar geometry of single polarization measurements performed on the same kinds of DRs deposited on glass, with, in addition, an atomic force microscope (AFM) mounted on an inverted microscope to probe the single DRs orientation, it has been recently evidenced that the maximum of fluorescence was obtained for a polarization parallel to the single DRs axis.[24] Together with our observation of inplane dipoles parallel to the oily streaks stripes, this suggests that the DRs axis is itself oriented parallel to the stripes. DRs are thus perpendicular to the 8CB anchoring direction, but parallel to the 8CB hemicylinder axis and thus parallel to the expected edge dislocations of oily streaks. Smectic dislocations are characterized by a disordered linear core of high energy with a diameter of the order of a few nanometers.[59] The DRs width (with a total of 7 nm) matches the one of the smectic dislocation cores. In addition to their elongated shape, this size matching promotes their trapping inside the line defects, in agreement with the previously evidenced phenomenon of nanospheres trapping by topological LC defects.[60–63] The induced orientation of the DRs, parallel to the dislocation cores (Figure 1), may correspond to a precise localization of the DRs within the disordered cores. This localization of DRs within and parallel to the dislocation core indeed maximizes the volume of disordered liquid crystal expelled by the DRs and thus decreases the disorder energy of the smectic liquid crystal film in the presence of dislocations. If we consider elementary smectic dislocations, their energy per unit of length has been measured in free standing 8CB smectic films to be 0.5 kT Å^{-1}.[64] A single DR of length l = 23 nm, trapped in the dislocation core and

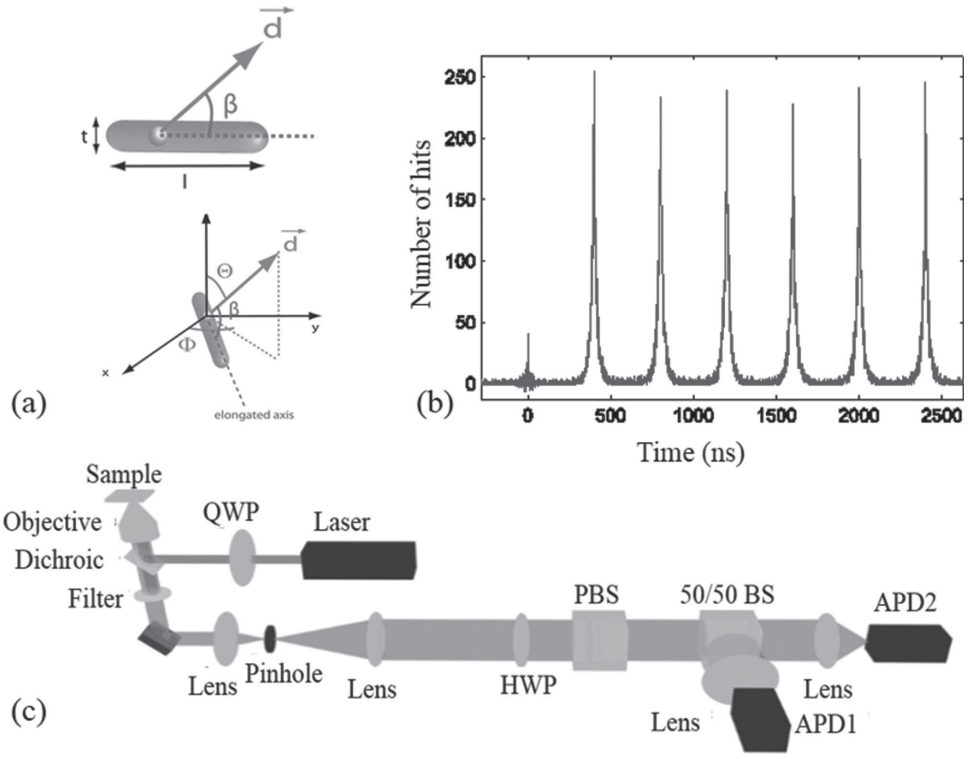

Figure 5. a) Schematic of the DRs with the angle β between the DR *c*-axis and the emitting dipole indicated, together with the out-of-plane tilt of the dipole, θ, and the inplane tilt, Φ. b) Autocorrelation function for a typical DR in 8CB, with 8CB background contribution (see Figure S1, Supporting Information) subtracted following Ref. [69]. c) Experimental setup during the polarization measurement.

parallel to its axis, allows to decrease the liquid crystal disorder energy by 115 kT, leading to a significant advantage for the liquid crystal film. The DRs, once trapped in smectic dislocations, may be particularly well-stabilized. Only motion of the DRs along the dislocations cores may occur, in agreement with experimental observations. Our results may consequently correspond to DRs, trapped within the liquid crystal dislocations, parallel to the substrate and parallel to the 8CB stripes.

The origin of this nanorod-induced orientation is obviously different from the one induced in nematics, this latter being driven by the anchoring of liquid crystal molecules at the DR surface, usually leading to DRs oriented parallel to the nematic director.[39,40] In contrast, in smectic oily streaks, the induced orientation is parallel to the dislocations, thus perpendicular to the liquid crystal director. Generally speaking, if the nanorod diameter is small enough to avoid, outside the dislocations core, a new smectic distortion/disorder energy larger than the energy advantage associated with the nanorod presence in the dislocation core, we expect no liquid crystal-induced aggregation.[45] As a consequence, contrary to the nematic case, the liquid crystal anchoring at the DR surface is also expected to have almost no influence and the DRs may be efficiently oriented by the dislocation, independently of the liquid crystal anchoring at their surface. This appears in agreement with the fact that nanospheres surrounded by different ligands, alkylthiols, are similarly linearly oriented, since they form chains parallel to the dislocations in the 8CB oily streaks.[65]

If the DR axis is parallel to the smectic dislocations, an out-of-plane tilt of the DR dipole corresponds to an emitting dipole tilted by an angle β (see **Figure 5**a) from the horizontal nanorod axis, in agreement with Ref. [51]. In presence of a β angle between the fixed DR axis and the dipole, we anticipate a free rotation of the dipole around the DR.[51] In contrast, Figures 1 and 3 suggest that the dipoles remain all oriented in the plane defined by the rod and the normal to the substrate. The origin of such a strictly induced out-of-plane dipole orientation is not clear. Surface charges may exist on these DRs, related either to the crystallographic orientation of the nanorod surface[66] or/and to dangling bonds unsaturated by the surface ligands.[67] A symmetry breaking in the smectic phase at the DR interface may occur, due to the charges at the DR surface, which may orient all neighboring 8CB molecular dipoles. Strong electric dipolar interactions between the 8CB molecular dipoles (4.9 D)[68] and the DR dipoles may thus favor DR dipole orientation in the plane parallel to the 8CB stripes and perpendicular to the substrate. This outstanding property of the smectic oily streaks evidences a good control of single emitters since, with our smectic liquid crystal/DRs composites, we create a dispersion of single-photon emitters of controlled polarization phase, oriented along a unique direction for one given sample. It opens the way to macroscopic nanoemitter lines, sources of well polarized single-photon emission. Generally speaking, the ability to orient nanorods shows a high potential of the smectic oily streaks for the control of nanoparticles' optical properties. This goes well beyond semiconducting nanoparticles, being, for example, well adapted for inducing anisotropic plasmonic extinction of metallic nanorods.

4. Conclusion

In conclusion, we showed that the oily streak structure created by a liquid crystal deposited on a rubbed polymer induces an alignment along a unique direction of the DRs diluted in the liquid crystal matrix, leading to fixed orientation for the emitting in-plane dipoles. This has been shown at the single particle level thanks to the evidence of the intensity second-order autocorrelation function of each DR. Over a collection of DRs, we found the fluorescence polarization orientations to be along the liquid crystal stripes within an 8° standard deviation. The DRs used in this study thus behave as individual polarized single-photon emitters. This orientation along the oily streaks axis is likely due to the trapping of the DRs within the smectic dislocation cores, oriented along a single direction, together with electric dipole–dipole interactions between the DRs dipoles and the liquid crystal molecules. This leads to an orientation of the DRs without aggregation, a priori independently of the ligand's nature around the DRs. This work thus shows the feasibility of a large-scale orientation of anisotropic emitters without the stringent requirements shown in previous studies (control of the ligand's nature, continuity of the sample, particles in direct contact with each other, or under the influence of an external electric field). The experiment demonstrates the trapping efficiency of smectic dislocations which not only trap but also align elongated nano-objects, along a single direction for a given sample, thanks to the use of rubbed polymer substrates. These results open the way for not only orienting dot-in-rods but also for creating chains of oriented dot-in-rods emitting polarized light.

5. Experimental Section

Colloidal core/shell CdSe/CdS DRs were synthesized by using a seeded growth approach.[18] They are constituted of a CdSe core with a diameter of 2.9 nm and surrounded by a rod-like CdS shell (Figure 5a). As confirmed by transmission electron microscopy (TEM) analysis, they present a rod-like shape with an average length $l = 23 \pm 3$ nm and a total thickness $t \approx 7$ nm (Figure S2, Supporting Information). The relatively large thickness is responsible for an increased photostability and blinking suppression with respect to thin shell DRs, grown with standard techniques.[7] They are surrounded by organic ligands, namely, TOP (trioctylphosphine) and ODPA (octadecylphosphonic acid).

Solid surfaces consisting of a glass substrate with spin-coated and rubbed polyvinyl alcohol polymer (PVA) of thickness 10 nm were used as substrate to realize films of a smectic liquid crystal composed of elongated molecules of 4-*n*-octyl-4′-cyanobiphenyl (8CB). Drops (40 µL) of a 8CB solution in toluene (2×10^{-1} M), containing DRs (10^{-13} mol), were spin-coated on top of rubbed PVA-coated substrates at 4000 rpm during 30 s with an acceleration varying between 200 and 300 rpm s^{-1}. This results in 8CB films of thickness varying between 100 and 200 nm, where arrays of parallel stripes were visualized by optical microscopy (Figure 2a).

On PVA rubbed surfaces, a planar anchoring of the liquid crystalline molecules is induced at the interface with the PVA, while a perpendicular (homeotropic) alignment is produced at the air interface. Such an anchoring antagonism leads to distortions of the smectic films (Figure 2b), commonly named smectic "oily streaks" for film thicknesses in the range 100–300 nm.[55,70,71] The smectic layers become curved, stacking on top of each other to form flattened hemicylinders of axis parallel to the substrate and perpendicular to the anchoring orientation, the latter being defined by the PVA rubbing direction (Figure 2a,b). The corresponding hemicylinders' periodicity and orientation can be determined by optical microscopy since they are associated with straight linear stripes in the pictures (Figure 2a). Oily streaks are associated with several highly distorted areas (Figure 2b): i) the curvature walls, W, between neighboring hemicylinders underlined in red in Figure 2b,[55] ii) the region connecting the flattened hemicylinders to the substrate with a straight grain boundary,[71] and iii) the area around the rotation axis *C*. This area has been shown on MoS_2 crystalline substrates[72] and rubbed PVA polymer[71] to be formed by a rotating grain boundary, to remove the most curved smectic layers. These grain boundaries connecting different number of smectic layers from each side can be composed of a number of straight dislocations parallel to the hemicylinder axis.[71–73] Smectic dislocations are linear topological defects, made of elastically deformed smectic layers around a linear core defect with a diameter of the order of the smectic layer width, i.e., ≈ 3 nm for 8CB.[59] The linear cores are expected to behave as efficient traps for nanoparticles. It has been shown that gold nanoparticles and quantum dots can be trapped in oily streaks, leading to the formation of straight chains of nanoparticles, parallel to the dislocations.[65]

A confocal fluorescence microscopy setup (Figure 5c) was used with either a mercury lamp or a laser diode source to excite single DRs. The emitted light was collected by avalanche photodiodes or a CCD camera. To first observe the liquid crystal on the substrate as well as to locate the DRs, a mercury lamp with a filter selecting the 436 nm line was used to illuminate the sample. The light reflected at the interface between the liquid crystal and the glass substrate confirms the presence of the oily streaks (Figure 2a). To locate the DRs themselves, we used a high-pass filter with a 570 nm cutoff in the detection path, eliminating the reflection from the liquid crystal while allowing the photoluminescence signal from the DRs to get through (wavelength between 575 and 650 nm).

A circularly polarized picosecond pulsed laser diode (λ = 404 nm, repetition rate 2.5 MHz) was then focused on each single DR embedded in the liquid crystal (average optical index 1.57) through a high numerical aperture air objective (NA = 0.95). As light absorption efficiency of a DR depends on the polarization of the excitation light,[39,51] the chosen circular polarization ensures a comparable excitation for DRs with potentially different orientations, allowing similar emission intensities for all particles. Low excitation power below the DR absorption saturation level was used in order to limit multiexciton emission and blinking.[7] In a first step, intensity second-order autocorrelation at zero delay measurements ($g^2(0)$) were performed with a Hanbury–Brown and Twiss setup consisting of a 50/50 beam-splitter (BS), separating the photon flow to two avalanche photodiodes and measuring the coincidence counts. The corresponding antibunching is shown in Figure 5b, with the 8CB background fluorescence independently measured and subtracted as explained in Ref. [69] (see Supporting Information). The peak at zero delay, although not fully absent (probably due to weak multiexciton emission), is much lower than the other peaks, to select the isolated ones for further measurements and which indicates that we are observing a single isolated DR. It allows to establish that all the measured DRs are single-photon emitters. In a second step, a rotating linear polarizer made of a half-wave plate (HWP) and a polarizing beam splitter (PBS) was placed before the 50/50 BS (Figure 1c). The rotation of the half-wave plate allowed the analysis of the polarized component of the beam emitted by each isolated DR. 90 s-long time traces were registered with the half-wave plate rotating at a constant speed of 1° s^{-1}. Representative results of this measurement are reported in Figure 1c for typical raw data.

By virtue of their peculiar emission diagram[6] and the generally high level of emitted linear polarization, measured both through ensemble and single particle spectroscopy,[5,24,25,57,58] DRs are commonly associated with 1D linear dipoles.[7,25,69]

In spherical coordinates with *z*-axis referred as the microscope optical axis (axis perpendicular to the substrate), the orientation of a dipole can be marked out by its in-plane Φ and out-of plane θ angles (Figure 5a). Its emission intensity as a function of the analysis angle α is expressed as[52]

$$I(\alpha) = I_{min} + (I_{max} - I_{min})\cos^2(\Phi - \alpha) \quad (1)$$

where I_{max} (resp. I_{min}) corresponds to the maximum (resp. minimum) intensity when α is varied. They depend on the out-of-plane angle θ, on the numerical aperture of the collecting objective and on the environment of the dipole. The angle α itself is the polarization rotation angle caused by the $\lambda/2$ plate (rotated by an angle $\alpha/2$). Its origin has been calibrated by measuring the signal received when the emitted light is replaced by a known polarized signal. The 0° has been defined by the maximum of intensity for a polarization parallel to the Ox axis of the optical microscopy pictures (see Figure 1a,b). The detected intensity is maximum when α equals to the in-plane angle of the dipole $\Phi \pm \pi$. Thereby, Equation (1) allows the assessment of Φ, giving thorough knowledge of the in-plane orientation of each individual DR dipole.

Supporting Information

Supporting Information is available from the Wiley Online Library or from the author.

Acknowledgements

The authors would like to thank Dominique Demaille and Francis Breton. For financial support, they would also like to thank the Agence Nationale de la Recherche (P3N Delight, JCJC Ponimi, and PNano Nanodiellipso), the programs C'nano NanoPlasmAA and C'Nano Sophopol, the PUF program of the French Embassy in the United States of America.

Received: September 24, 2014
Revised: January 14, 2015
Published online: February 6, 2015

[1] M. D. Eisaman, J. Fan, A. Migdall, S. V. Polyakov, *Rev. Sci. Instrum.* **2011**, *82*, 071101.
[2] A. Shabaev, A. L. Efros, *Nano Lett.* **2004**, *4*, 1821.
[3] R. Krahne, G. Morello, A. Figuerola, C. George, S. Deka, L. Manna, *Phys. Rep.* **2011**, *501*, 75.
[4] X. Chen, A. Nazzal, D. Goorskey, M. Xiao, Z. A. Peng, X. G. Peng, *Phys. Rev. B* **2001**, *64*, 245304.
[5] D. V. Talapin, R. Koeppe, S. Gotzinger, A. Kornowski, J. M. Lupton, A. L. Rogach, O. Benson, J. Feldmann, H. Weller, *Nano Lett.* **2003**, *3*, 1677.
[6] F. Pisanello, L. Martiradonna, G. Leménager, P. Spinicelli, A. Fiore, L. Manna, J.-P. Hermier, R. Cingolani, E. Giacobino, M. De Vittorio, A. Bramati, *Appl. Phys. Lett.* **2010**, *96*, 033101.
[7] F. Pisanello, G. Lemenager, L. Martiradonna, L. Carbone, S. Vezzoli, P. Desfonds, P. D. Cozzoli, J. P. Hermier, E. Giacobino, R. Cingolani, M. De Vittorio, A. A. Bramati, *Adv. Mater.* **2013**, *25*, 1974.
[8] A. Qualtieri, F. Pisanello, M. Grande, T. Stomeo, L. Martiradonna, G. Epifani, A. Fiore, A. Passaseo, M. De Vittorio, *Microelectron. Eng.* **2010**, *87*, 1435.
[9] F. Pisanello, A. Qualtieri, T. Stomeo, L. Martiradonna, R. Cingolani, A. Bramati, M. De Vittorio, *Opt. Lett.* **2010**, *35*, 1509.
[10] C. H. Bennett, G. Brassard, *Proc. IEEE Int. Conf. Comput., Syst. Signal Process.* **1984**, *175*, 8.
[11] Y. Amit, A. Faust, I. Lieberman, L. Yedidya, U. Banin, *Phys. Status Solidi A* **2012**, *209*, 235.
[12] A. Ghezelbash, B. Koo, B. A. Korgel, *Nano Lett.* **2006**, *6*, 1832.
[13] L. S. Li, A. P. Alivisatos, *Phys. Rev. Lett.* **2003**, *90*, 097402.
[14] M. Artemyev, B. Moller, U. Woggon, *Nano Lett.* **2003**, *3*, 509.
[15] L. S. Li, J. Walda, L. Manna, A. P. Alivisatos, *Nano Lett.* **2002**, *2*, 557.
[16] C. Querner, M. D. Fischbein, P. A. Heiney, M. Drndi , *Adv. Mater.* **2008**, *20*, 2308.
[17] D. V. Talapin, E. V. Shevchenko, C. B. Murray, A. Kornowski, S. Forster, H. Weller, *J. Am. Chem. Soc.* **2004**, *126*, 12984.
[18] L. Carbone, C. Nobile, M. De Giorgi, F. D. Sala, G. Morello, P. Pompa, M. Hytch, E. Snoeck, A. Fiore, I. R. Franchini, M. Nadasan, A. F. Silvestre, L. Chiodo, S. Kudera, R. Cingolani, R. Krahne, L. Manna, *Nano Lett.* **2007**, *7*, 2942.
[19] A. Rizzo, C. Nobile, M. Mazzeo, M. De Giorgi, A. Fiore, L. Carbone, R. Cingolani, L. Manna, G. Gigli, *ACS Nano* **2009**, *3*, 1506.
[20] P. Yang, F. Kim, *ChemPhysChem* **2002**, *3*, 503.
[21] S. Gupta, Q. L. Zhang, T. Emrick, T. P. Russell, *Nano Lett.* **2006**, *6*, 2066.
[22] K. J. Wu, K. C. Chu, C. Y. Chao, Y. F. Chen, C. W. Lai, C. C. Kang, C. Y. Chen, P. T. Chou, *Nano Lett.* **2007**, *7*, 1908.
[23] Z. Hu, M. D. Fischbein, C. Querner, M. Drndić, *Nano Lett.* **2006**, *6*, 2585.
[24] I. Hadar, G. B. Hitin, A. Sitt, A. Faust, U. Banin, *J. Phys. Chem. Lett.* **2013**, *4*, 502.
[25] B. T. Diroll, T. Dadosh, A. Koschitzky, Y. Goldman, C. B. Murray, *J. Phys. Chem. C* **2013**, *117*, 23928.
[26] C. Knorowski, A. Travesset, *EPL* **2012**, *100*, 56004.
[27] K. Thorkelsson, J. H. Nelson, A. P. Alivisatos, T. Xu, *Nano Lett.* **2013**, *13*, 4908.
[28] R. A. M. Hikmet, P. T. K. Chin, D. V. Talapin, H. Weller, *Adv. Mater.* **2005**, *17*, 1436.
[29] F. A. Aldaye, A. L. Palmer, H. F. Sleiman, *Science* **2008**, *321*, 1795.
[30] V. Georgakilas, D. Gournis, V. Tzitzios, L. Pasquato, D. M. Guldi, M. Prato, *J. Mater. Chem.* **2007**, *17*, 2679.
[31] H. Qi, T. Hegmann, *J. Mater. Chem.* **2008**, *18*, 3288.
[32] O. Stamatoiu, J. Mirzaei, X. Feng, T. Hegmann, *Top. Curr. Chem.* **2012**, *318*, 331.
[33] H. K. Bisoyi, S. Kumar, *Chem. Soc. Rev.* **2011**, *40*, 306.
[34] J. P. F. Lagerwall, G. Scalia, *Curr. Appl. Phys.* **2012**, *12*, 1387.
[35] J. Mirzaei, M. Reznikov, T. Hegmann, *J. Mater. Chem.* **2012**, *22*, 22350.
[36] C. Blanc, D. Coursault, E. Lacaze, *Liq. Cryst. Rev.* **2013**, *1*, 83.
[37] J. M. Winkler, S. G. Lukishova, L. J. Bissell, *J. Phys.: Conf. Ser.* **2013**, *414*, 012006.
[38] S. G. Lukishova, A. W. Schmid, R. Knox, P. Freivald, L. J. Bissell, R. W. Boyd, C. R. Stroud, K. L. Marshall, *J. Mod. Opt.* **2007**, *54*, 417.
[39] S. V. Burylov, Y. L. Raikher, *Phys. Lett. A* **1990**, *149*, 279.
[40] S. V. Burylov, Y. L. Raikher, *Phys. Rev. E* **1994**, *50*, 358.
[41] Q. Liu, Y. Cui, D. Gardner, X. Li, S. He, I. I. Smalyukh, *Nano Lett.* **2010**, *10*, 1347.
[42] S. Umadevi, F. Xiang, T. Hegmann, *Adv. Funct. Mater.* **2013**, *23*, 1393.
[43] O. Buluy, S. Nepijko, V. Reshetnyak, E. Ouskova, V. Zadorozhnii, A. Leonhardt, M. Ritschel, G. Schönhense, Y. Reznikov, *Soft Matter* **2011**, *7*, 644.
[44] M. R. Thomas, S. Klein, R. J. Greasty, S. Mann, A. W. Perriman, R. M. Richardson, *Adv. Mater.* **2012**, *24*, 4424.
[45] J. S. Pendery, O. Merchiers, D. Coursault, J. Grand, H. Ayeb, R. Greget, B. Donnio, J.-L. Gallani, C. Rosenblatt, N. Félidj, Y. Borensztein, E. Lacaze, *Soft Matter* **2013**, *9*, 9366.
[46] M. V. Mukhina, V. V. Danilov, A. O. Orlova, M. V. Fedorov, M. V. Artemyev, A. V. Baranov, *Nanotechnology* **2012**, *23*, 325201.
[47] Q. Liu, Y. Yuan, I. I. Smalyukh, *Nano Lett.* **2014**, *14*, 4071.
[48] A. L. Rodarte, C. G. L. Ferri, C. Gray, L. S. Hirst, S. Ghosh, *Proc. SPIE* **2012**, *8279*, 82790H.
[49] H. S. Chen, C. W. Chen, C. H. Wang, F. C. Chu, C. Y. Chao, C. C. Kang, P. T. Chou, Y. F. Chen, *J. Phys. Chem. C* **2010**, *114*, 7995.

[50] V. V. Danilov, M. V. Artem'ev, A. V. Baranov, G. M. Ermolaeva, N. A. Utkina, A. I. Khrebtov, *Opt. Spectrosc.* **2008**, *105*, 37.
[51] C. Lethiec, F. Pisanello, L. Carbone, A. Bramati, L. Coolen, A. Maître, *New J. Phys.* **2014**, *16*, 093014.
[52] C. Lethiec, J. Laverdant, H. Vallon, C. Javaux, B. Dubertret, C. Schwob, L. Coolen, A. Maître, *Phys. Rev. X* **2014**, *4*, 021037.
[53] M. Böhmer, J. Enderlein, *J. Opt. Soc. Am. B* **2003**, *20*, 554.
[54] D. Patra, I. Gregor, J. Enderlein, *J. Phys. Chem. A* **2004**, *108*, 6836.
[55] J. P. Michel, E. Lacaze, M. Alba, M. Gailhanou, M. de Boissieu, M. Goldmann, *Phys. Rev. E* **2004**, *70*, 011709.
[56] J. T. Hu, L. S. Li, W. D. Yang, L. Manna, L. W. Wang, A. P. Alivisatos, *Science* **2001**, *292*, 2060.
[57] B. T. Diroll, A. Koschitzky, C. B. Murray, *J. Phys. Chem. Lett.* **2014**, *5*, 85.
[58] A. Sitt, A. Salant, G. Menagen, U. Banin, *Nano Lett.* **2011**, *11*, 2054.
[59] M. Kleman, *Points, Lines, and Walls: In Liquid Crystals, Magnetic Systems, and Various Ordered Media*, John Wiley & Sons Inc., New York **1977**.
[60] H. Yoshida, Y. Tanaka, K. Kawamoto, H. Kubo, T. Tsuda, A. Fujii, S. Kuwabata, H. Kikuchi, M. Ozabi, *Appl. Phys. Exp.* **2009**, *2*, 121501.
[61] B. Rozic, V. Tzitzios, E. Karatairi, U. Tkalec, G. Nounesis, Z. Kutnjak, G. Cordoyiannis, R. Rosso, E. G. Virga, I. Musevic, S. Kralj, *Eur. Phys. J. E* **2011**, *34*, 17.
[62] B. Senyuk, J. S. Evans, P. J. Ackerman, T. Lee, P. Manna, L. Vigderman, E. R. Zubarev, J. van de Lagemaat, I. I. Smalyukh, *Nano Lett.* **2012**, *12*, 955.
[63] G. Cordoyiannis, V. S. R. Jampani, S. Kralj, S. Dhara, V. Tzitzios, G. Basina, G. Nounesis, Z. Kutnjak, C. S. P. Tripathi, P. Losada-Perez, D. Jesenek, C. Glorieux, I. Muševič, A. Zidansek, H. Ameinitsch, J. Thoen, *Soft Matter* **2013**, *9*, 3956.
[64] J.-C. Géminard, C. Laroche, P. Oswald, *Phys. Rev. E* **1998**, *58*, 5923.
[65] D. Coursault, J. Grand, B. Zappone, H. Ayeb, G. Levi, N. Felidj, E. Lacaze, *Adv. Mater.* **2012**, *24*, 1461.
[66] R. Krishnan, M. A. Hahn, Z. Yu, J. Silcox, P. M. Fauchet, T. D. Krauss, *Phys. Rev. Lett.* **2004**, *92*, 216803.
[67] J. Müller, J. M. Lupton, A. L. Rogach, J. Feldmann, D. V. Talapin, H. Weller, *Phys. Rev. B* **2005**, *72*, 205339.
[68] K. Gueu, E. Megnassan, A. Proutiere, *Mol. Cryst. Liq. Cryst.* **1986**, *132*, 303.
[69] C. Vion, P. Spinicelli, L. Coolen, J. M. Frigerio, J. P. Hermier, A. Maître, *Opt. Express* **2012**, *18*, 7440.
[70] B. Zappone, E. Lacaze, *Phys. Rev. E* **2008**, *78*, 061704.
[71] D. Coursault, B. H. Ibrahim, L. Pelliser, B. Zappone, A. de Martino, E. Lacaze, B. Gallas, *Opt. Express* **2014**, *22*, 23182.
[72] J. P. Michel, E. Lacaze, M. Goldmann, M. Gailhanou, M. de Boissieu, M. Alba, *Phys. Rev. Lett.* **2006**, *96*, 027803.
[73] C. Williams, M. Kléman, *J. Phys. Coll.* **1975**, *36*, 315.